nature chemical biology

ARTICLES

https://doi.org/10.1038/s41589-018-0120-6

O-GlcNAc modification of eIF4GI acts as a translational switch in heat shock response

Xingqian Zhang[1], Xin Erica Shu[1,2] and Shu-Bing Qian[1,2]*

Heat shock response (HSR) is an ancient signaling pathway leading to thermoprotection of nearly all living organisms. Emerging evidence suggests that intracellular O-linked β-*N*-acetylglucosamine (*O*-GlcNAc) serves as a molecular 'thermometer' by reporting ambient temperature fluctuations. Whether and how *O*-GlcNAc modification regulates HSR remains unclear. Here we report that, upon heat shock stress, the key translation initiation factor eIF4GI undergoes dynamic *O*-GlcNAcylation at the N-terminal region. Without *O*-GlcNAc modification, the preferential translation of stress mRNAs is impaired. Unexpectedly, stress mRNAs are entrapped within stress granules (SGs) that are no longer dissolved during stress recovery. Mechanistically, we show that stress-induced eIF4GI *O*-GlcNAcylation repels poly(A)-binding protein 1 and promotes SG disassembly, thereby licensing stress mRNAs for selective translation. Using various eIF4GI mutants created by CRISPR/Cas9, we demonstrate that eIF4GI acts as a translational switch via reversible *O*-GlcNAcylation. Our study reveals a central mechanism linking heat stress sensing, protein remodeling, SG dynamics and translational reprogramming.

Dynamic glycosylation of proteins with *O*-GlcNAc has been rapidly emerging as a cellular signaling mechanism[1–3]. The reversible *O*-GlcNAcylation is mediated by a single pair of enzymes: *O*-GlcNAc transferase (OGT) and *O*-GlcNAcase (OGA). While the former installs *O*-GlcNAc on serine or threonine residues of proteins[4], the latter removes the monosaccharide unit from proteins[5]. The dynamic cycling of *O*-GlcNAc modification occurs in a nutrient- and stress-responsive manner. For many ectotherms, *O*-GlcNAc levels are closely correlated with ambient temperature during their development[6]. Likewise, heat shock stress rapidly increases the levels of *O*-GlcNAcylation in mammalian cells[7–9]. Notably, *O*-GlcNAc modification has been shown to confer heat stress resistance in endotherms such as humans[10]. However, neither the identity of protein targets nor the physiological significance of stress-induced *O*-GlcNAcylation has been clearly defined.

HSR is an evolutionarily conserved pathway that results in rapid induction of genes encoding molecular chaperones essential for protection and recovery from cellular damages[11–13]. Upon heat shock stress, there is a marked inhibition of global protein synthesis accompanied by the selective induction of stress proteins such as Hsp70 (also termed Hsp72). This reprogramming of gene expression involves a coordination of transcription[14], translation[15] and post-transcriptional processes[16,17]. Additionally, a wide variety of stress stimuli trigger the assembly of SGs, discrete RNA–protein structures that contain nontranslating mRNAs[18–21]. SGs have been proposed to affect mRNA translation and stability and have been linked to cellular processes such as apoptosis. Assembly and disassembly of SGs are modulated by various post-translational modifications, as well as numerous protein-remodeling complexes[21]. However, very little is known about mRNA triage during SG formation. Whether there is a common mechanism underlying SG dynamics and selective mRNA translation remains elusive.

In this study, we investigated the mechanistic linkage between *O*-GlcNAc modification and HSR in mammalian cells. We uncovered a functional switch for eIF4GI that relies on *O*-GlcNAc modification to couple selective mRNA translation and SG dynamics. These findings provide fundamental insights into SG regulation and generate new perspectives for translational control of HSR.

Results

Deficient Hsp70 translation in cells lacking OGT. In mammalian cells, *O*-GlcNAc modification has been implicated in HSR, although the underlying mechanism remains to be resolved[6,10]. We took advantage of a mouse embryonic fibroblast (MEF) cell line, $Ogt^{F/Y}$(mER-Cre) MEFs, carrying an *Ogt* gene that can be excised by simple administration of 4-hydroxytamoxifen (4HT)[10]. As expected, 48 h exposure to 4HT resulted in complete depletion of OGT and disappearance of background *O*-GlcNAc (Fig. 1a). Upon heat shock stress, a robust induction of Hsp70 was evident in MEFs before 4HT treatment. However, OGT depletion via 4HT pretreatment led to marked attenuation of Hsp70 induction (Fig. 1a). The impairment in Hsp70 expression was not due to the side effect of 4HT, as the same treatment had little effect in control MEFs bearing GFP (Supplementary Fig. 1a). Additionally, OGT depletion did not yet lead to apoptosis or necrosis, at least under these experimental conditions (Supplementary Fig. 1b,c). The OGT-dependent Hsp70 induction also held true in HeLa cells, as RNA interference (RNAi)-mediated OGT knockdown reduced Hsp70 levels (Supplementary Fig. 1d). The crucial role of OGT in HSR is not limited to Hsp70, because small chaperones such as Hsp25 also showed substantial reduction in stressed MEFs lacking OGT (Supplementary Fig. 1e). However, constitutively expressed chaperones such as Hsc70 were minimally affected.

Looking into the underlying mechanism, we found that OGT depletion had negligible effect on Hsp70 mRNA levels in heat-stressed MEFs (Fig. 1a). To assess the translational status of Hsp70 in these cells, we examined mRNA enrichment in polysome fractions separated by sucrose gradient sedimentation[22]. The stress-induced Hsp70 mRNA, but not the housekeeping messenger *B2m*, showed decreased polysome enrichment after OGT depletion (Fig. 1b). These results suggest a crucial role for OGT in translational control of HSR.

[1]Division of Nutritional Sciences, Cornell University, Ithaca, NY, USA. [2]Graduate Program in Nutritional Sciences, Cornell University, Ithaca, NY, USA.
*e-mail: sq38@cornell.edu

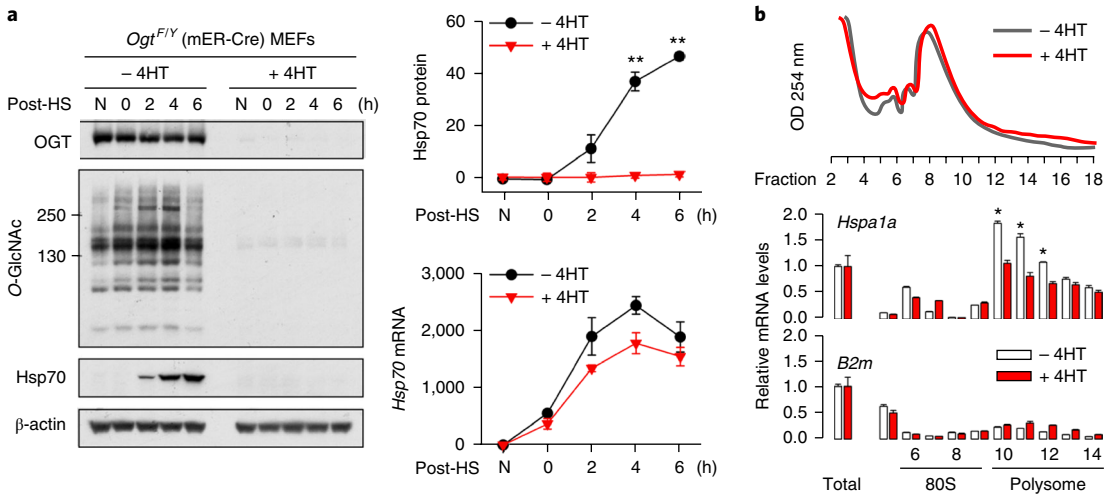

Fig. 1 | Cells lacking OGT exhibit deficient Hsp70 translation. a, *Ogt*$^{F/Y}$(mER-Cre) MEFs were pretreated with (+) or without (–) 0.5 μM 4HT for 24 h followed by normal medium for another 24 h. Cells were heat stressed (HS) at 42 °C for 1 h and recovered at 37 °C for indicated times. Whole-cell lysates were collected for immunoblotting and total mRNAs extracted for RT-qPCR. N: no heat shock. Top right: relative protein levels quantified by densitometry and normalized to β-actin. Bottom right: relative levels of Hsp70 mRNA normalized to β-actin. Basal values in wild-type cells are set to 1. Error bars, mean ± s.e.m.; $^{**}P < 0.01$; two-way ANOVA; $n = 3$ independent experiments; uncropped blots are shown in Supplementary Fig. 9. **b**, MEF cells as in **a** were heat stressed at 42 °C for 1 h and recovered at 37 °C for 2.5 h. Whole-cell lysates were collected for polysome profile analysis as shown in the top panel. Total RNA was extracted from individual polysome fractions followed by RT-qPCR measuring β2 microglobulin (*B2m*) and Hsp70 (*Hspa1a*) mRNA. Relative mRNA levels are normalized to the total. OD, optical density. Error bars, mean ± s.e.m.; $^{*}P < 0.05$; two-way ANOVA; $n = 3$ independent experiments.

Heat shock stress induces *O*-GlcNAcylation of eIF4GI. We next attempted to identify protein targets subjected to *O*-GlcNAc modification in response to heat shock stress. We initially focused on ribosomal proteins, whose *O*-GlcNAcylation has been reported previously[23,24]. However, translating ribosomes exhibited very low basal levels of *O*-GlcNAc modification and showed negligible changes in response to heat shock stress (Supplementary Fig. 2a,b). We noticed that the most conspicuous *O*-GlcNAc species in ribosome fractions were of high molecular weight, and they disappeared in OGT-depleted MEF cells after 4HT pretreatment (Supplementary Fig. 2b,c). A close inspection of these high-molecular-weight species revealed a distinct band of approximate 250 kDa that emerged shortly after heat shock stress (Fig. 2a). Notably, the heat-stress-induced *O*-GlcNAc species appeared earlier than Hsp70 and vanished during stress recovery. This dynamic feature was reproducible in HeLa cells (Fig. 2a), suggesting that the reversible *O*-GlcNAc modification is a general phenomenon in mammalian cells upon heat shock stress.

Given the putative role of *O*-GlcNAcylation in translational control of HSR, we surveyed several translation initiation factors that are relatively large in size. eIF4GI emerged as one of the candidates because of high scores of predicted *O*-GlcNAcylation and the similar size of 250 kDa on gels (Supplementary Fig. 3a). To experimentally validate this finding, we immunoprecipitated endogenous eIF4GI from HeLa cells with or without heat shock stress. With similar input levels, eIF4GI obtained from heat-stressed cells showed a marked increase in *O*-GlcNAc signal (Fig. 2b). We also examined the eIF4GI paralog eIF4GII[25], which appeared to be barely modified in spite of the same size and sequence homology (Supplementary Fig. 3b). The stress-induced *O*-GlcNAc modification of eIF4GI was further confirmed in MEF cells (Fig. 2c). Notably, OGT depletion after 4HT treatment completely abolished *O*-GlcNAc signals associated with eIF4GI. Therefore, heat shock stress triggers rapid *O*-GlcNAc modification of eIF4GI.

We next applied tandem mass spectrometry (MS) to map the positions of *O*-GlcNAc modification on endogenous eIF4GI purified from heat-stressed MEF cells. With a peptide coverage of 67.5%, MS revealed only one modification site with high confidence, Ser68 (Fig. 2d). Notably, Ser68 in the mouse eIF4GI is well conserved in the human eIF4GI (annotated as Ser61). The Ser61 of human eIF4GI has previously been mapped as a putative modification site[26]. To validate the identified modification site, we cloned the full-length eIF4GI from HeLa cells and fused YFP and Flag to the N terminus. Stress-induced *O*-GlcNAc modification was well preserved in transfected YFP-flag-eIF4GI (Fig. 2e). Introducing an S68A mutation completely abolished *O*-GlcNAc signals from purified eIF4GI fusion proteins (Fig. 2e). By contrast, S1285A mutation minimally affected the total *O*-GlcNAc levels of transfected eIF4GI. Therefore, the Ser68 is the primary site of eIF4GI that undergoes dynamic *O*-GlcNAcylation in response to heat shock stress.

eIF4GI *O*-GlcNAcylation repels PABP1. The N-terminal third of eIF4GI contains binding sites for poly(A)-binding protein 1 (PABP1) and eIF4E[27,28]. We found that eIF4GI bound to eIF4E irrespective of *O*-GlcNAc modification (Fig. 3a). Notably, heat stress diminished the interaction between eIF4GI and PABP1 in wild-type cells. However, in MEF cells lacking OGT, comparable amount of PABP1 molecules were pulled down by eIF4GI before and after stress (Fig. 3a). Given the close proximity of Ser68 and the PABP1 binding site of eIF4GI, the stress-induced PABP1 dissociation is likely to be due to stress-induced *O*-GlcNAcylation of eIF4GI. To test this possibility, we conducted reciprocal immunoprecipitation by purifying either eIF4E or PABP1 followed by eIF4GI detection. While eIF4E readily pulled down both modified and unmodified eIF4GI, much less eIF4GI was coprecipitated with PABP1 and showed no *O*-GlcNAc signals (Fig. 3b). Notably, heat shock stress also diminished the coprecipitation between PABP1 and eIF4E. As an independent validation, we treated MEF cells with thiamet G, an inhibitor of OGA. Consistent with the dynamic nature of eIF4GI *O*-GlcNAcylation, we observed an increase of *O*-GlcNAc signals during the early stage of stress recovery (3 h) but an evident decrease at the late stage (6 h) (Supplementary Fig. 3c). In the presence of thiamet G, however, the *O*-GlcNAc modification of eIF4GI was sustained. Notably, much less PABP1 was

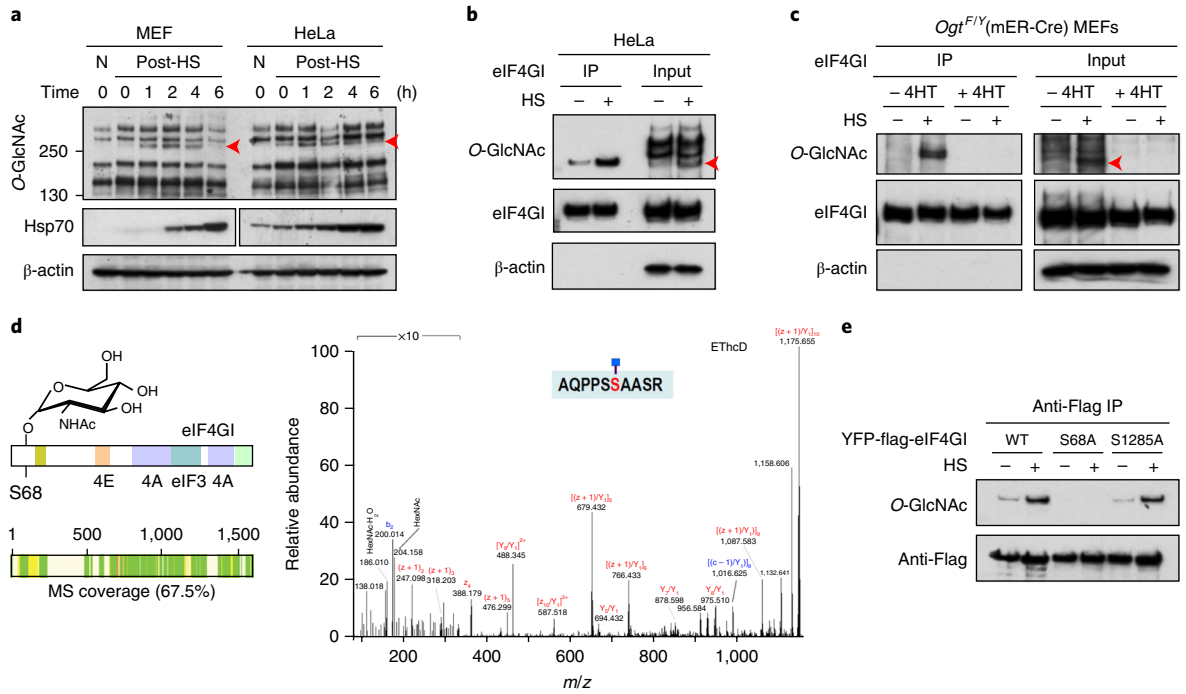

Fig. 2 | eIF4GI undergoes dynamic *O*-GlcNAcylation in response to heat shock stress. a, *Ogt*$^{F/Y}$(mER-Cre) MEFs and HeLa cells were heat stressed (HS) at 42 °C for 1 h and recovered at 37 °C for the indicated times. Whole-cell lysates were collected for immunoblotting. N: no heat shock. Red arrowhead: putative *O*-GlcNAcylated eIF4GI. Representative results are shown from three independent experiments. Uncropped blots are shown in Supplementary Fig. 9. **b**, HeLa cells were heat stressed at 42 °C for 1 h and recovered at 37 °C for 2.5 h. Cell lysates were immunoprecipitated (IP) using an anti-eIF4GI antibody followed by immunoblotting. Representative results are shown from three independent experiments. Uncropped blots are shown in Supplementary Fig. 9. **c**, *Ogt*$^{F/Y}$(mER-Cre) MEFs were heat stressed at 42 °C for 1 h and recovered at 37 °C for 2.5 h. Cell lysates were immunoprecipitated using an anti-eIF4GI antibody followed by immunoblotting. Representative results are shown from three independent experiments. Uncropped blots are shown in Supplementary Fig. 9. **d**, Left: the schematic structure of eIF4GI with main domains color-coded for different protein interactions. Right: immunoprecipitated eIF4GI from heat-stressed MEF cells as in **c** was subjected to mass spectrometry. An electron transfer/higher energy collision dissociation (EThcD) MS/MS spectrum of m/z 587.7913^{2+} identifies *O*-GlcNAcylation of Ser68 (red), illustrated along the peptide sequence shown at top. HexNAc, *N*-acetylhexoseamine. **e**, MEF cells were transfected with plasmids expressing YFP-flag-tagged eIF4GI wild type (WT) or mutants for 24 h. Transfected cells were heat stressed at 42 °C for 1 h and recovered at 37 °C for 4 h. Cell lysates were immunoprecipitated using an anti-Flag antibody followed by immunoblotting. Representative results are shown from three independent experiments. Uncropped blots are shown in Supplementary Fig. 9.

coprecipitated with eIF4GI (Supplementary Fig. 3c). Therefore, stress-induced *O*-GlcNAc modification of eIF4GI remodels the assembled eIF4F complex by dissociating PABP1.

PABP1 is believed to bring the 5′ cap and 3′ end of mRNA into a closed loop and stimulate the cap-dependent translation initiation[29,30]. It is conceivable that, by opening the mRNA loop, *O*-GlcNAcylation of eIF4GI not only represses cap-dependent translation, but also facilitates cap-independent translation by remodeling the eIF4F complex. Since eIF4GI bears an inherent mRNA binding capacity[31], we speculated that stress-induced *O*-GlcNAcylation led to preferential binding of eIF4GI to stress mRNAs for selective translation. To illustrate the mRNA-binding properties of eIF4GI with or without *O*-GlcNAc modification, we enriched eIF4GI-associated mRNAs by zero-distance cross-linking followed by real-time quantitative qPCR (RT-qPCR) (Fig. 3c). In control MEF cells, heat shock stress led to sixfold enrichment of Hsp70 (*Hspa1a*) mRNA to eIF4GI, but not β-actin (*Actb*) mRNA. Surprisingly, and perhaps counterintuitively, OGT depletion resulted in about 25-fold enrichment of *Hspa1a* mRNA in association with eIF4GI (Fig. 3c). Since eIF4GI lacking *O*-GlcNAc modification does not support *Hspa1a* mRNA translation (Fig. 1), the stable interaction between the unmodified eIF4GI and mRNA is suggestive of nonproductive trapping. As an independent validation, we compared the mRNA-binding properties of YFP-flag-eIF4GI and the S68A mutant in transfected MEF cells. As expected, reduced PABP1 binding upon heat shock stress was only observed for the wild-type eIF4GI but not the S68A mutant (Supplementary Fig. 3d). In agreement with the endogenous eIF4GI results, a large amount of mRNA was significantly enriched in the S68A mutant in comparison to the wild type (Fig. 3d). This unexpected result suggests that stress-induced *O*-GlcNAcylation of eIF4GI releases stress mRNAs that otherwise are trapped.

eIF4GI *O*-GlcNAcylation promotes SG disassembly. We noticed that, upon heat shock stress, less eIF4GI was recovered from the soluble fraction in MEF cells lacking OGT (Fig. 3a, input). Fractionation analysis further confirmed this feature (Fig. 4a). In addition to eIF4GI, eIF4E and PABP1 also reduced their solubility in OGT-null cells upon heat shock stress. This feature is reminiscent of stress granule (SG) formation in the cytoplasm[32]. Immunofluorescence indeed revealed more cytoplasmic puncta signified by SG markers in OGT knockout cells than in wild-type MEFs after heat shock stress (Fig. 4b). In wild-type cells, heat-stress-induced SGs were transient and quickly resolved during stress recovery. In OGT knockout cells, however, the SG puncta largely remained even after the cessation of stress for 2 h (Supplementary Fig. 4a). To substantiate this finding further, we knocked down OGT in HeLa cells and observed a sustained formation of SGs during stress recovery (Supplementary Fig. 4b). Therefore, lack of *O*-GlcNAcylation results in delayed SG clearance during stress recovery.

The unanticipated role of *O*-GlcNAc in SG disassembly is in sharp contrast to the results of a previous study that reported that OGT

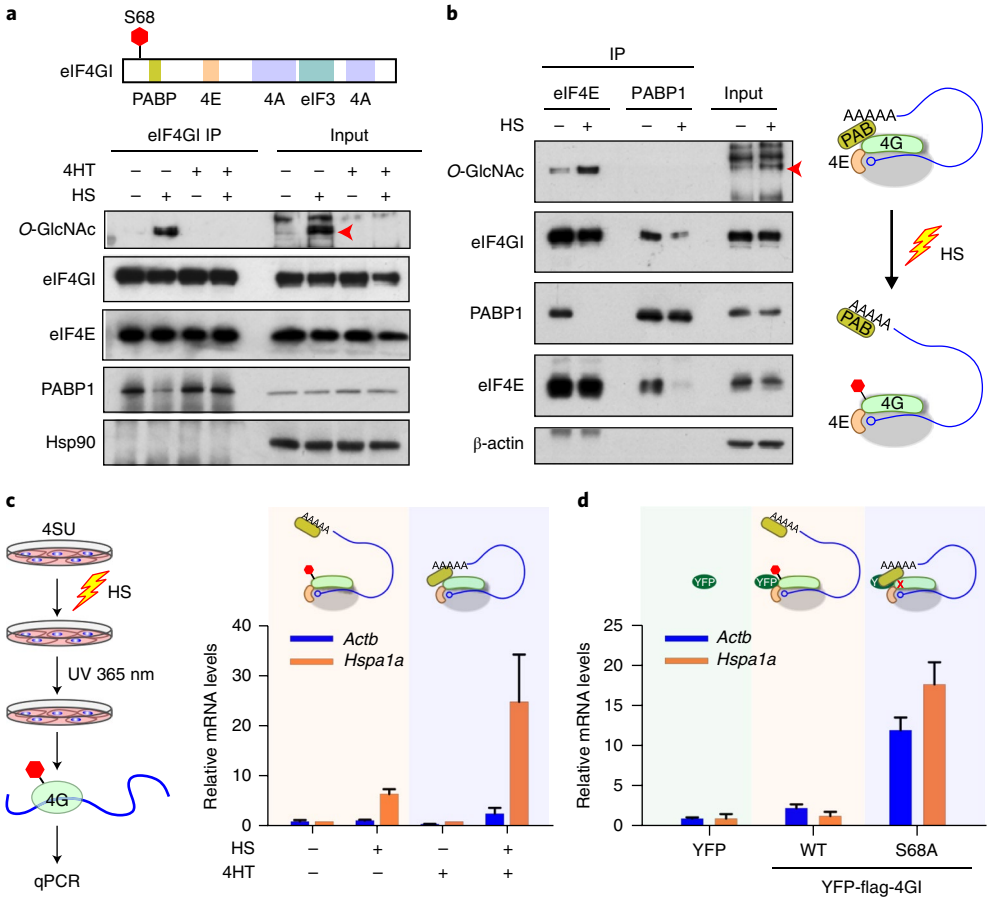

Fig. 3 | eIF4GI *O*-GlcNAcylation repels PABP1. a, $Ogt^{F/Y}$(mER-Cre) MEFs were heat stressed (HS) at 42 °C for 1 h and recovered at 37 °C for 2.5 h. Cell lysates were immunoprecipitated (IP) using an anti-eIF4GI antibody followed by immunoblotting. Representative results are shown from three independent experiments. Uncropped blots are shown in Supplementary Fig. 9. **b**, Left: HeLa cells were heat stressed at 42 °C for 1 h and recovered at 37 °C for 2.5 h. Cell lysates were immunoprecipitated using an anti-eIF4E or anti-PABP1 antibodies followed by immunoblotting. Representative results are shown from three independent experiments. Uncropped blots are shown in Supplementary Fig. 9. Right: a schematic of eIF4F complexes. 4E, eIF4E; 4G, eIF4GI; PAB, PABP1. **c**, $Ogt^{F/Y}$(mER-Cre) MEFs were treated with 100 μM 4-thiouridine (4SU) followed by heat stress at 42 °C for 1 h and recovered at 37 °C for 2.5 h. Cells were then irradiated with UV at 365 nm and cell lysates were immunoprecipitated using an anti-eIF4GI antibody. Immunoprecipitates were treated with proteinase K followed by RNA extraction and RT-qPCR. Basal levels of both transcripts in wild-type cells (−HS, −4HT) are set to 1. Error bars, mean ± s.e.m.; $n = 3$ independent experiments. **d**, MEF cells were transfected with plasmids expressing YFP-flag-tagged eIF4GI wild type (WT) or mutant (S68A) for 24 h. Transfected cells were treated with 100 μM 4SU followed by heat stress at 42 °C for 1 h and recovered at 37 °C for 2.5 h. Cells were then irradiated at 365 nm UV and cell lysates were immunoprecipitated using an anti-Flag antibody. Immunoprecipitates were treated with proteinase K followed by RNA extraction and RT-qPCR. YFP was used as a negative control. Basal levels of both transcripts in wild-type cells (−HS, −4HT) are set to 1. Error bars, mean ± s.e.m.; $n = 3$ independent experiments.

was essential for SG assembly[24]. To directly address this issue, we assessed SG formation in MEF cells with or without OGT knockout after exposure to sodium arsenite, a potent SG inducer used in the previous study. Sodium arsenite treatment readily triggered SG formation in both wild-type and OGT knockout cells (Supplementary Fig. 5a). In addition, HeLa cells with OGT knockdown also exhibited a comparable number of, if not more, SG puncta upon sodium arsenite exposure (Supplementary Fig. 5b). We conclude that OGT is dispensable for SG formation. In the case of heat shock stress, *O*-GlcNAcylation of eIF4GI appears to be essential in SG disassembly, presumably by promoting selective translation of Hsp70[33]. Indeed, adding back Hsp70 into OGT knockout cells via recombinant adenoviruses prevented the sustained SG formation induced by heat stress (Supplementary Fig. 6).

eIF4GI *O*-GlcNAcylation releases stress mRNAs from SGs. Stress mRNAs such as *Hspa1a* are largely excluded from SG recruitment, likely because of their preferential translation under stress conditions[18–20]. Having observed defective Hsp70 synthesis and the marked mRNA trapping by eIF4GI in the absence of *O*-GlcNAc modification, we reasoned that these stress mRNAs were likely to be retained within SGs. To test this possibility, we used fluorescence in situ hybridization (FISH) to detect the cellular location of *Hspa1a* induced by heat shock stress[16]. In wild-type MEFs, FISH signals distributed uniformly in the cytoplasm, as well as nuclear foci that accounted for active Hsp70 transcription (Fig. 4c). In MEFs lacking OGT, however, the cytoplasmic FISH signals formed clear puncta overlapping with SG markers such as G3BP1. Therefore, in the absence of *O*-GlcNAcylation, *Hspa1a* mRNA is largely entrapped within SGs.

To confirm that it is the modification of eIF4GI that contributes to the mRNA triage in SG dynamics, we compared SG induction in MEF cells transfected with YFP-flag-eIF4GI or the S68A mutant. In spite of the presence of endogenous eIF4GI, overexpression of the nonmodifiable S68A mutant was sufficient for sustained SG formation in response to heat shock

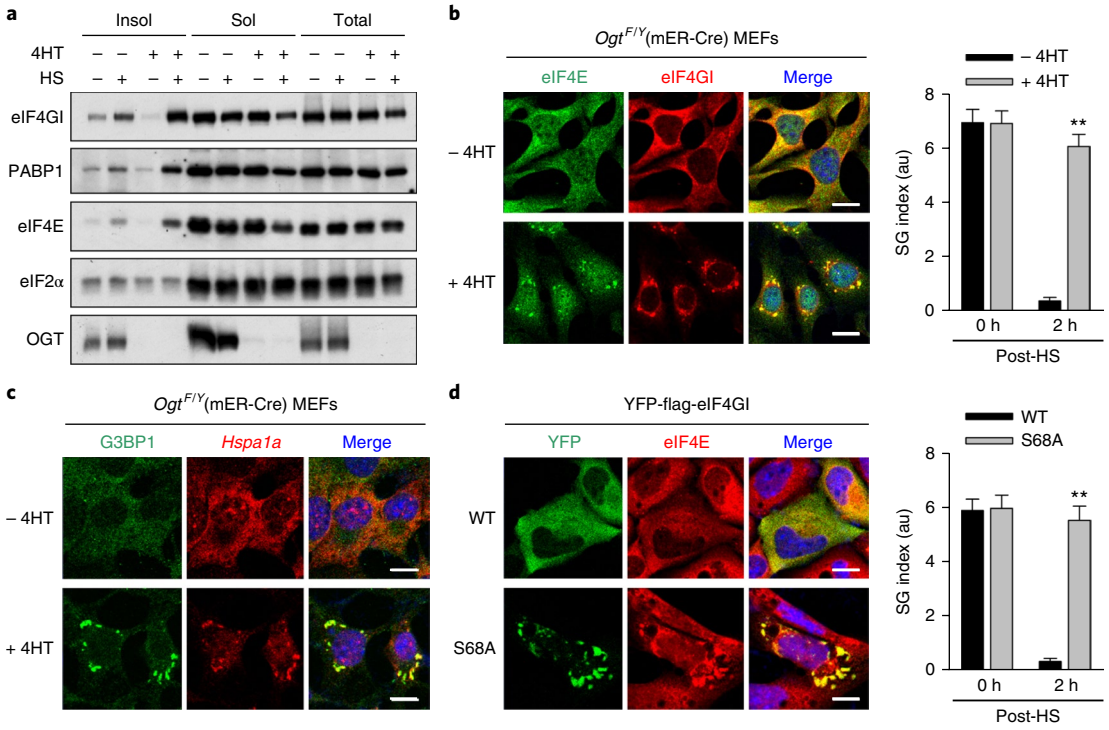

Fig. 4 | Depletion of *O*-GlcNAcylation from eIF4GI prevents SG disassembly. a, $Ogt^{F/Y}$(mER-Cre) MEFs were heat stressed (HS) at 42 °C for 1 h and recovered at 37 °C for 2 h. Whole-cell lysates were fractionated into soluble (Sol; supernatant) and insoluble (Insol; pellet) fractions by centrifugation at 16,000 *g* for 15 min at 4 °C. Both fractions and total samples were collected for immunoblotting. Representative results are shown from three independent experiments. Uncropped blots are shown in Supplementary Fig. 9. **b**, $Ogt^{F/Y}$(mER-Cre) MEFs were heat stressed at 42 °C for 1 h and recovered at 37 °C for 2 h. Cells were fixed with 3.7% formaldehyde followed by immunofluorescence staining. Scale bars, 10 μm. Right: SGs were quantified by defining an index (SG area/cell area) based on eIF4GI immunofluorescence. Data are presented as arbitrary units (au). Error bars indicate mean ± s.e.m. for at least three independent experiments in which four fields of view with at least 30 cells per field of view were quantified. $^{**}P < 0.01$; two-way ANOVA. **c**, $Ogt^{F/Y}$(mER-Cre) MEFs were heat stressed at 42 °C for 1 h and recovered at 37 °C for 2.5 h. Cells were then fixed with 3.7% formaldehyde followed by simultaneous G3BP1 immunofluorescence staining and *Hspa1a* FISH. Scale bars, 10 μm. Representative cells are shown from among 120 cells. **d**, MEF cells were transfected with plasmids expressing YFP-flag-tagged eIF4GI wild type (WT) or mutant (S68A) for 24 h. Transfected cells were heat stressed at 42 °C for 1 h and recovered at 37 °C for 4 h. Cells were fixed with 3.7% formaldehyde followed by immunofluorescence staining. Scale bars, 10 μm. Right: SG index based on YFP. Error bars indicate mean ± s.e.m. for at least three independent experiments in which 120 YFP-positive cells were quantified. $^{**}P < 0.01$; two-way ANOVA.

stress (Fig. 4d). Additionally, the cytoplasmic puncta formed by the eIF4GI mutant contained strong FISH signals for *Hspa1a* (Supplementary Fig. 5c). These results demonstrate the dominant-negative feature of eIF4GI mutants lacking *O*-GlcNAc modification. It also suggests that stress-induced *O*-GlcNAcylation of eIF4GI tends to liberate stress mRNAs from SGs, thereby permitting selective translation.

eIF4GI *O*-GlcNAcylation controls SG dynamics via PABP1. OGT targets hundreds of cellular proteins for *O*-GlcNAcylation[1,2]. It is unclear whether the modification status of eIF4GI alone is sufficient to influence SG dynamics, as well as selective mRNA translation in response to heat stress. To address this question, we used the CRISPR/Cas9 system to genetically engineer the endogenous *Eif4g1*. In mammals, the *Eif4g1* gene gives rise to five documented isoforms via alternative promoters, splice sites and start codons[34]. These eIF4GI variants can be resolved by prolonged gel electrophoresis (Fig. 5a). *O*-GlcNAc enrichment from heat-stressed cells followed by eIF4GI blotting revealed only the largest two isoforms (Fig. 5a, right), further suggesting that it is the N-terminal region of eIF4GI that undergoes *O*-GlcNAcylation in response to heat shock stress. OGT has been reported to mediate site-specific protein cleavage, as exemplified by host cell factor-1 (HCF-1)[35]. In MEFs lacking OGT, however, the abundance of eIF4GI isoforms remained unchanged (Supplementary Fig. 7a).

Relying on a single guide RNA (sgRNA) targeting Ser67 and Ser68 (Supplementary Fig. 7b), we established several MEF cell lines harboring different *Eif4g1* mutations. As expected, the majority of mutants exhibited an insert/deletion (indel) that resulted in frameshift of *Eif4g1*. For instance, in a cell line bearing a single A insertion before the Ser67 codon, very little full-length eIF4GI was detectable (Fig. 5b). Intriguingly, the short isoforms of eIF4GI became more abundant in these cells, presumably as a result of cellular adaptation. Since the physiological eIF4GI short isoforms lack the N-terminal region for *O*-GlcNAc modification, they offers a valuable tool for assessing the functionality of eIF4GI lacking both *O*-GlcNAc modification and PABP1 binding. Despite the absence of full-length eIF4GI, the induction of Hsp70 synthesis upon heat shock stress remained robust in these cells (Fig. 5b). However, these eIF4GI short isoforms neither changed their solubility nor supported SG formation upon heat shock stress (Fig. 5d,e). Thus, eIF4GI–PABP1 interaction is crucial for SG formation but dispensable for selective Hsp70 synthesis.

To confirm the critical role of PABP1 in SG induction, we assessed SG formation in MEF cells with PABP1 knockdown. Remarkably, even partial depletion of PABP1 nearly abolished SG assembly upon heat shock stress (Supplementary Fig. 8a). However, there was little effect on stress-induced Hsp70 synthesis (Supplementary Fig. 8b). The PABP1-independent Hsp70 translation is in agreement with the notion that the selective translation of stress mRNAs occurs preferentially during heat stress recovery.

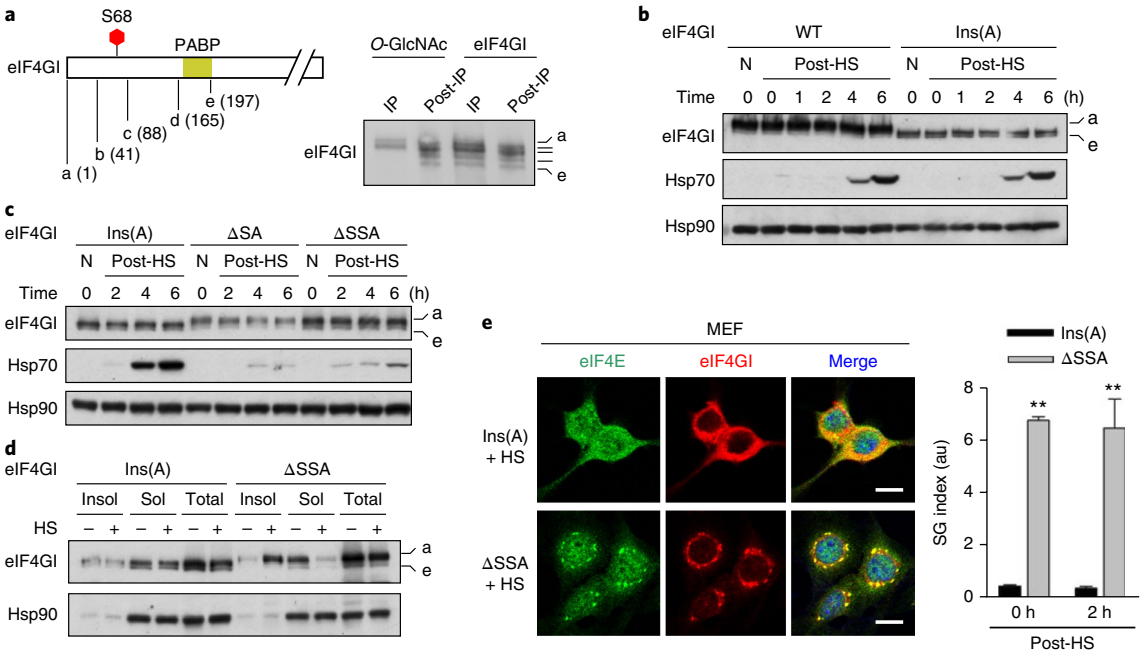

Fig. 5 | The N terminus of eIF4GI acts a functional switch via *O*-GlcNAcylation. a, Left: N-terminal region of eIF4GI showing possible isoforms, with the number in parentheses indicating the position of the first amino acid. Both the *O*-GlcNAc modification site S68 and the PABP1 binding domain are highlighted. Right: eIF4GI isoforms obtained from heat-stressed MEF cells before and after immunoprecipitation (IP) using either *O*-GlcNAc or eIF4GI antibodies. Representative results are shown from three independent experiments. Uncropped blots are shown in Supplementary Fig. 9. **b**, Genomically engineered MEF cells bearing wild type (WT) or A insertion (Ins(A)) mutant eIF4GI were heat stressed (HS) at 42 °C for 1 h and recovered at 37 °C for indicated times. Whole-cell lysates were collected for immunoblotting. Representative results are shown from three independent experiments. Uncropped blots are shown in Supplementary Fig. 9. N: no heat shock. **c**, Genomically engineered MEF cells bearing the eIF4GI Ins(A) mutant or a deletion mutant (ΔSA and ΔSSA) were heat stressed at 42 °C for 1 h and recovered at 37 °C for indicated times. Whole-cell lysates were collected for immunoblotting. Uncropped blots are shown in Supplementary Fig. 9. **d**, Genomically engineered MEF cells bearing the eIF4GI Ins(A) mutant or a deletion mutant (ΔSSA) were heat stressed at 42 °C for 1 h and recovered at 37 °C for 2 h. Whole-cell lysates were fractionated into soluble (Sol; supernatant) and insoluble (Insol; pellet) fractions by centrifugation at 16,000 *g* for 15 min at 4 °C. Both fractions and total samples were collected for immunoblotting. Uncropped blots are shown in Supplementary Fig. 9. **e**, Genomically engineered MEF cells bearing the eIF4GI Ins(A) mutant or a deletion mutant (ΔSSA) were heat stressed at 42 °C for 1 h and recovered at 37 °C for 2.5 h. Cells were fixed with 3.7% formaldehyde followed by immunofluorescence staining. Scale bars, 10 μm. Right: SG index based on eIF4GI immunostaining. Error bars indicate mean ± s.e.m. for at least three independent experiments in which four fields of view with at least 30 cells per field of view were quantified. $^{**}P < 0.01$; two-way ANOVA.

We next attempted to establish MEF cell lines with genomic in-frame *Eif4g1* mutations in order to generate full-length eIF4GI that maintains the PABP1 binding capacity but cannot be modified by *O*-GlcNAc. Among hundreds of cell clones created by CRISPR/Cas9, two eIF4GI mutants lacking Ser68 (ΔSA and ΔSSA) were successfully selected (Supplementary Fig. 7b). Unlike the frame-shifting Ins(A) mutant, the in-frame deletion mutants showed predominantly full-length eIF4GI (Fig. 5c). As expected, both ΔSSA and Ins(A) mutants showed no discernable *O*-GlcNAc signals upon heat shock stress (Supplementary Fig. 8c). With the intact PABP1 interaction, the eIF4GI ΔSSA mutant quickly lost solubility upon heat shock stress and readily formed SG puncta (Fig. 5d,e). More critically, stress-induced Hsp70 synthesis was severely impaired in these cells (Fig. 5c). Therefore, SG disassembly and selective mRNA translation proceed in a coordinated manner during stress recovery from heat shock.

***O*-GlcNAcylation acts as a functional switch for eIF4GI.** To substantiate the finding that the *O*-GlcNAcylation of eIF4GI acts as a functional switch between SG induction and selective mRNA translation, we conducted rescue experiments. To deplete endogenous eIF4GI variants, we introduced indel mutations into *Eif4g1* by targeting the conserved downstream region (P700) using CRISPR/Cas9 (Supplementary Fig. 7b). All surviving cells still contained residual eIF4GI but failed to induce robust Hsp70 synthesis in response to heat shock stress (Supplementary Fig. 8d). This result indicates that other eIF4G homologs, such as eIF4GII and DAP5[36], could not compensate for the eIF4GI loss of function in selective translation of *Hspa1a* mRNA. Notably, lack of eIF4GI completely prevented heat-stress-induced SG formation (Supplementary Fig. 8e). We then reintroduced different variants of eIF4GI, including the shortest isoform, M197, which lacks the PABP1 binding site and a truncated variant, M457, which lacks the entire N-terminal region (Fig. 6a). To prevent downstream initiation of these transgenes, we blocked their N termini by fusing a YFP module. We also introduced synonymous mutations into these constructs rendering them resistant to sgRNA targeting P700. All the constructs except the S68A mutant restored stress-induced Hsp70 synthesis (Fig. 6a). However, adding back M197 or M457 mutants failed to trigger SG induction upon heat shock stress (Fig. 6b). Despite the relatively low expression levels in transfected cells, both M197 and M457 mutants rescued Hsp70 synthesis as fully as the wild type. Therefore, an intact PABP1 binding site is not essential for selective translation of Hsp70. In fact, a persistent PABP1 association (as in the case of the S68A mutant) prevents subsequent stress mRNA translation. Further supporting the crucial role of *O*-GlcNAcylation in the functional switch of eIF4GI, only the wild-type eIF4GI was able to rescue both SG formation and Hsp70 synthesis (Fig. 6a,b).

A model emerges from our data: the dynamic interaction between eIF4GI and PABP1 serves as a regulatory key to SG

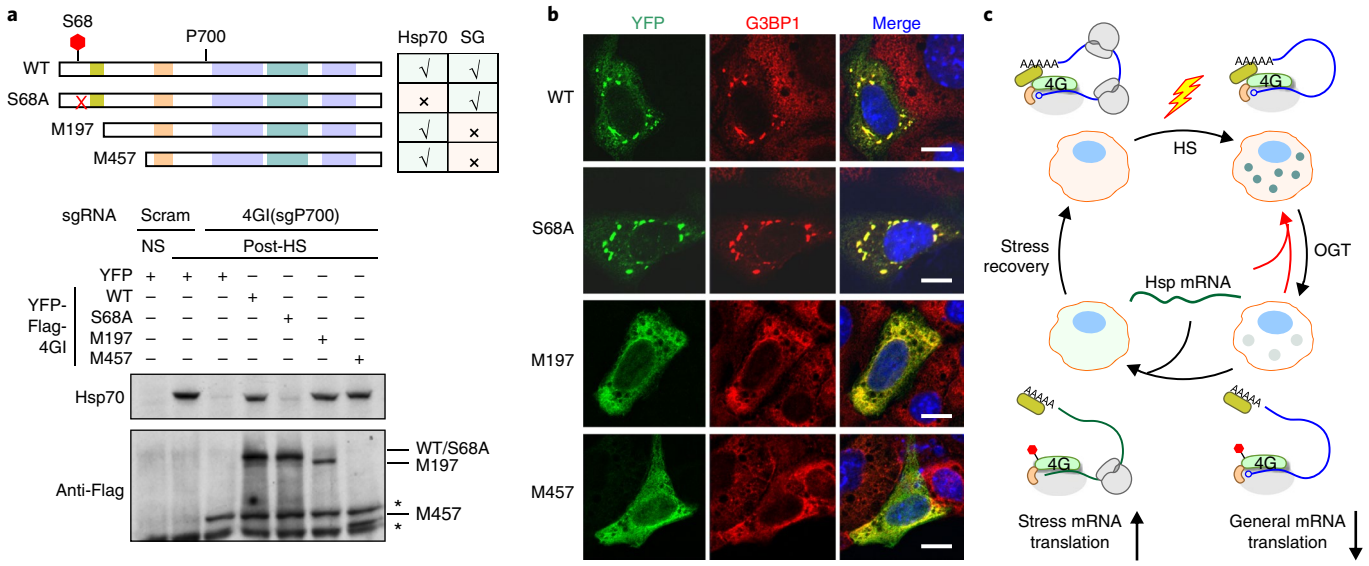

Fig. 6 | Rescuing effects of eIF4GI variants in SG dynamics and Hsp70 synthesis. a, Genomically engineered MEF cells with eIF4GI knockdown mediated by sgRNA targeting P700 were transfected with plasmids expressing eIF4GI wild type (WT), S68A mutants or short isoforms (M197 or M457). Cells were heat stressed (HS) 24 h after transfection at 42 °C for 1 h and recovered at 37 °C for 2.5 h. Top: eIF4G variants and summary of their rescuing effects in Hsp70 synthesis and SG formation. Bottom: immunoblotting results using whole-cell lysates from transfected cells with heat stress and 6 h recovery. Representative results are shown from three independent experiments. *, nonspecific bands. Uncropped blots are shown in Supplementary Fig. 9. **b**, The same cells as used in **a** with G3BP1 staining immediately after heat shock treatment. Scale bars, 10 μm. Representative cells are shown from among 120 cells. **c**, A working model depicts the role of eIF4GI *O*-GlcNAcylation in functional switch between SG formation and selective translation. Persistent eIF4GI and PABP1 association promotes cap-dependent mRNA translation under the normal growth condition while triggering SG induction upon heat shock stress. Stress-induced *O*-GlcNAcylation of eIF4GI displaces PABP1, thereby dissolving SGs and permitting selective translation of stress mRNAs.

dynamics, as well as selective mRNA translation. Persistent eIF4GI and PABP1 association promotes cap-dependent mRNA translation under the normal growth condition while triggering SG induction upon heat-stress-induced translation arrest (Fig. 6c). Stress-induced *O*-GlcNAcylation of eIF4GI dissociates PABP1, thereby dissolving SGs followed by selective translation of stress mRNAs. Our data reveal a functional switch of eIF4GI that is controlled via reversible *O*-GlcNAcylation at the N terminus. By controlling direct PABP1 interaction, this dynamic modification of eIF4GI coordinates SG induction and selective translation of stress mRNAs.

Discussion

Environmental stress is detrimental to cell viability and requires an adequate reprogramming of cellular activities to maximize cell survival. Proteins that confer adaptive benefits are often preferentially synthesized; this is subject to extensive regulation at different levels. Dynamic *O*-GlcNAc modification has been shown to integrate environmental cues into a wide range of fundamental cellular processes, including transcription, protein degradation, basal metabolism and signaling pathways[1,2]. Our finding that dynamic *O*-GlcNAc modification acts as a functional switch for eIF4GI imparts an additional layer of regulation in maintaining protein homeostasis.

The initiation factor eIF4GI acts as a major hub in translational control of many cellular processes, stress response and viral infection[37]. The N-terminal region of eIF4GI, although largely unstructured, contains the PABP1 and eIF4E binding sites. PABP1 is known to enhance cap- and poly(A)-dependent mRNA translation via direct interaction with eIF4GI[29,30]. In heat-stressed cells, however, PABP1 is rapidly dissociated from eIF4GI. This feature is in line with the finding that selective translation of Hsp70 mRNA is neither cap- nor PABP1-dependent[15]. However, very little is known how PABP1 is evicted from the eIF4F complex during heat stress. We provide evidence that N-terminal *O*-GlcNAcylation of eIF4GI operates to remodel the initiation complex eIF4F. By displacing PABP1, the stress-induced *O*-GlcNAcylation of eIF4GI disrupts the closed mRNA loop. As a result, global protein synthesis remains repressed, whereas selective translation of stress mRNAs is permitted. Intriguingly, a wide range of viruses frequently target eIF4GI and PABP1, thereby subverting the host translation machinery[38,39]. For instance, the picornaviral 2 A protease cleaves eIF4G[40], whereas rotaviral NSP3 disrupts PABP1 and eIF4GI interaction[41]. Unlike the virus-mediated remodeling of eIF4F, which is long-lasting, stress-induced *O*-GlcNAc modification of eIF4GI is dynamic and reversible. This physiological switch enables cells to produce an adaptive translatome by turning on different modes of translation initiation in response to stress.

Perhaps the most surprising finding is that depleting *O*-GlcNAc modification or genetically eliminating the modification site of eIF4GI leads to mRNA trapping in the insoluble fraction. This paradoxical result is in accordance with the sustained SG formation in the absence of eIF4GI *O*-GlcNAcylation. SG formation is believed to be crucial for stress adaptation and is tightly coupled with the presence of mRNAs stalled in translation initiation[18–21]. Although both eIF4GI and PABP1 are core SG markers, it is intriguing to find that their interaction contributes to SG dynamics, at least during heat shock stress. A recent study reported that PABP1 in yeast (Pab1) mediates liquid–liquid phase separation in vivo and in vitro upon elevated temperatures[42]. However, SGs appear to form through the crosslinking of nontranslating mRNAs, which provide a scaffold or platform for multiple RNA-binding proteins[21]. Our findings echo the importance of mRNA conformation in SG assembly and disassembly. We propose that persistent eIF4GI–PABP1 interaction, when it is not engaged for active translation, readily poises the looped mRNA for SG formation in the cytoplasm. Disrupting eIF4GI–PABP1 association by either *O*-GlcNAc modification or deleting the N-terminal region of eIF4GI helps dissolve SGs. The identification of a single modification that toggles eIF4GI between inhibitors and drivers of SG assembly reshapes our current perceptions of SG regulation. Collectively, dynamic *O*-GlcNAcylation of

eIF4GI serves as a common mechanism underlying selective mRNA translation and SG dynamics. Since aberrant eIF4GI expression and dysregulated SG formation are associated with certain types of cancer and neurodegeneration[43–45], our findings raise the possibility that new strategies for converting functional variants of eIF4GI could be effective for treating these diseases.

Methods

Methods, including statements of data availability and any associated accession codes and references, are available at https://doi.org/10.1038/s41589-018-0120-6.

Received: 4 December 2017; Accepted: 10 July 2018;
Published online: 20 August 2018

References

1. Hardivillé, S. & Hart, G. W. Nutrient regulation of signaling, transcription, and cell physiology by O-GlcNAcylation. *Cell Metab.* **20**, 208–213 (2014).
2. Bond, M. R. & Hanover, J. A. A little sugar goes a long way: the cell biology of O-GlcNAc. *J. Cell Biol.* 208, (869–880 (2015).
3. Yang, X. & Qian, K. Protein O-GlcNAcylation: emerging mechanisms and functions. *Nat. Rev. Mol. Cell Biol.* **18**, 452–465 (2017).
4. Janetzko, J. & Walker, S. The making of a sweet modification: structure and function of O-GlcNAc transferase. *J. Biol. Chem.* **289**, 34424–34432 (2014).
5. Keembiyehetty, C. et al. Conditional knock-out reveals a requirement for O-linked *N*-acetylglucosaminase (O-GlcNAcase) in metabolic homeostasis. *J. Biol. Chem.* **290**, 7097–7113 (2015).
6. Radermacher, P. T. et al. O-GlcNAc reports ambient temperature and confers heat resistance on ectotherm development. *Proc. Natl Acad. Sci. USA* **111**, 5592–5597 (2014).
7. Groves, J. A., Lee, A., Yildirir, G. & Zachara, N. E. Dynamic O-GlcNAcylation and its roles in the cellular stress response and homeostasis. *Cell Stress Chaperones* **18**, 535–558 (2013).
8. Zachara, N. E. et al. Dynamic O-GlcNAc modification of nucleocytoplasmic proteins in response to stress. A survival response of mammalian cells. *J. Biol. Chem.* **279**, 30133–30142 (2004).
9. Martinez, M. R., Dias, T. B., Natov, P. S. & Zachara, N. E. Stress-induced O-GlcNAcylation: an adaptive process of injured cells. *Biochem. Soc. Trans.* **45**, 237–249 (2017).
10. Kazemi, Z., Chang, H., Haserodt, S., McKen, C. & Zachara, N. E. O-linked β-*N*-acetylglucosamine (*O*-GlcNAc) regulates stress-induced heat shock protein expression in a GSK-3β-dependent manner. *J. Biol. Chem.* **285**, 39096–39107 (2010).
11. Richter, K., Haslbeck, M. & Buchner, J. The heat shock response: life on the verge of death. *Mol. Cell* **40**, 253–266 (2010).
12. Bukau, B., Weissman, J. & Horwich, A. Molecular chaperones and protein quality control. *Cell* **125**, 443–451 (2006).
13. Morimoto, R. I. Regulation of the heat shock transcriptional response: cross talk between a family of heat shock factors, molecular chaperones, and negative regulators. *Genes Dev.* **12**, 3788–3796 (1998).
14. Anckar, J. & Sistonen, L. Regulation of HSF1 function in the heat stress response: implications in aging and disease. *Annu. Rev. Biochem.* **80**, 1089–1115 (2011).
15. Zhou, J. et al. Dynamic m^{6}A mRNA methylation directs translational control of heat shock response. *Nature* **526**, 591–594 (2015).
16. Vera, M. et al. The translation elongation factor eEF1A1 couples transcription to translation during heat shock response. *Elife* **3**, e03164 (2014).
17. Zander, G. et al. mRNA quality control is bypassed for immediate export of stress-responsive transcripts. *Nature* **540**, 593–596 (2016).
18. Buchan, J. R. & Parker, R. Eukaryotic stress granules: the ins and outs of translation. *Mol. Cell* **36**, 932–941 (2009).
19. Anderson, P. & Kedersha, N. Stress granules: the Tao of RNA triage. *Trends Biochem. Sci.* **33**, 141–150 (2008).
20. Cherkasov, V. et al. Coordination of translational control and protein homeostasis during severe heat stress. *Curr. Biol.* **23**, 2452–2462 (2013).
21. Protter, D. S. & Parker, R. Principles and properties of stress granules. *Trends Cell Biol* **26**, 668–679 (2016).
22. Sun, J., Conn, C. S., Han, Y., Yeung, V. & Qian, S. B. PI3K-mTORC1 attenuates stress response by inhibiting cap-independent Hsp70 translation. *J. Biol. Chem.* **286**, 6791–6800 (2011).
23. Zeidan, Q., Wang, Z., De Maio, A. & Hart, G. W. O-GlcNAc cycling enzymes associate with the translational machinery and modify core ribosomal proteins. *Mol. Biol. Cell* **21**, 1922–1936 (2010).
24. Ohn, T., Kedersha, N., Hickman, T., Tisdale, S. & Anderson, P. A functional RNAi screen links O-GlcNAc modification of ribosomal proteins to stress granule and processing body assembly. *Nat. Cell Biol.* **10**, 1224–1231 (2008).
25. Gradi, A. et al. A novel functional human eukaryotic translation initiation factor 4G. *Mol. Cell. Biol.* **18**, 334–342 (1998).
26. Wang, Z. et al. Extensive crosstalk between O-GlcNAcylation and phosphorylation regulates cytokinesis. *Sci. Signal.* **3**, ra2 (2010).
27. Sonenberg, N. & Dever, T. E. Eukaryotic translation initiation factors and regulators. *Curr. Opin. Struct. Biol.* **13**, 56–63 (2003).
28. Howard, A. & Rogers, A. N. Role of translation initiation factor 4G in lifespan regulation and age-related health. *Ageing Res. Rev.* **13**, 115–124 (2014).
29. Gallie, D. R. The cap and poly(A) tail function synergistically to regulate mRNA translational efficiency. *Genes Dev.* **5**, 2108–2116 (1991).
30. Preiss, T. & Hentze, M. W. Dual function of the messenger RNA cap structure in poly(A)-tail-promoted translation in yeast. *Nature* **392**, 516–520 (1998).
31. Yanagiya, A. et al. Requirement of RNA binding of mammalian eukaryotic translation initiation factor 4GI (eIF4GI) for efficient interaction of eIF4E with the mRNA cap. *Mol. Cell. Biol.* **29**, 1661–1669 (2009).
32. Jain, S. et al. ATPase-modulated stress granules contain a diverse proteome and substructure. *Cell* **164**, 487–498 (2016).
33. Walters, R. W., Muhlrad, D., Garcia, J. & Parker, R. Differential effects of Ydj1 and Sis1 on Hsp70-mediated clearance of stress granules in *Saccharomyces cerevisiae*. *RNA* **21**, 1660–1671 (2015).
34. Coldwell, M. J. & Morley, S. J. Specific isoforms of translation initiation factor 4GI show differences in translational activity. *Mol. Cell. Biol.* **26**, 8448–8460 (2006).
35. Capotosti, F. et al. *O*-GlcNAc transferase catalyzes site-specific proteolysis of HCF-1. *Cell* **144**, 376–388 (2011).
36. Liberman, N. et al. DAP5 associates with eIF2β and eIF4AI to promote Internal Ribosome Entry Site driven translation. *Nucleic Acids Res* **43**, 3764–3775 (2015).
37. Jackson, R. J., Hellen, C. U. & Pestova, T. V. The mechanism of eukaryotic translation initiation and principles of its regulation. *Nat. Rev. Mol. Cell Biol.* **11**, 113–127 (2010).
38. Walsh, D. & Mohr, I. Viral subversion of the host protein synthesis machinery. *Nat. Rev. Microbiol.* **9**, 860–875 (2011).
39. McCormick, C. & Khaperskyy, D. A. Translation inhibition and stress granules in the antiviral immune response. *Nat. Rev. Immunol.* **17**, 647–660 (2017).
40. Schneider, R. J. & Mohr, I. Translation initiation and viral tricks. *Trends Biochem. Sci.* **28**, 130–136 (2003).
41. Piron, M., Vende, P., Cohen, J. & Poncet, D. Rotavirus RNA-binding protein NSP3 interacts with eIF4GI and evicts the poly(A) binding protein from eIF4F. *EMBO J* **17**, 5811–5821 (1998).
42. Riback, J. A. et al. Stress-triggered phase separation is an adaptive, evolutionarily tuned response. *Cell* **168**, 1028–1040.e1019 (2017).
43. Silvera, D., Formenti, S. C. & Schneider, R. J. Translational control in cancer. *Nat. Rev. Cancer* **10**, 254–266 (2010).
44. Grabocka, E. & Bar-Sagi, D. Mutant KRAS enhances tumor cell fitness by upregulating stress granules. *Cell* **167**, 1803–1813.e1812 (2016).
45. Truitt, M. L. & Ruggero, D. New frontiers in translational control of the cancer genome. *Nat. Rev. Cancer* **16**, 288–304 (2016).

Acknowledgements

We thank N. E. Zachara for providing inducible MEF *Ogt* knockout cell lines. We also thank Qian lab members for discussions. We are grateful to Cornell University Life Sciences Core Laboratory Center for confocal microscope imaging support and mass spectrometry. We thank the Proteomic and MS Facility of Cornell University for providing the mass spectrometry data. The Orbitrap Fusion mass spectrometer was supported by US National Institutes of Health SIG grant 1S10 OD017992-01. This work was supported by grants to S.-B.Q. from the US National Institutes of Health (R01AG042400 and R01GM1222814) and a HHMI Faculty Scholar grant (55108556).

Author contributions

X.Z. and S.-B.Q conceived the project and designed the experiments. X.Z. performed the majority of experiments. X.E.S. assisted the experiments of eIF4GI isoforms and different chaperones in OGT knockout cells. S.-B.Q wrote the manuscripts. All authors discussed the results and edited the manuscript.

Competing interests

The authors declare no competing interests.

Additional information

Supplementary information is available for this paper at https://doi.org/10.1038/s41589-018-0120-6.

Reprints and permissions information is available at www.nature.com/reprints.

Correspondence and requests for materials should be addressed to S.-B.Q.

Publisher's note: Springer Nature remains neutral with regard to jurisdictional claims in published maps and institutional affiliations.

Methods

Cell lines and reagents. $Ogt^{F/Y}$(mER-Cre) and $Ogt^{F/Y}$(GFP) MEFs were kindly provided by Natasha E. Zachara (The Johns Hopkins University School of Medicine) and were maintained in Dulbecco's Modified Eagle's Medium (DMEM) with 10% FBS. For heat shock treatment, MEF cells were incubated at 42 °C water bath for 1 h followed by recovery at 37 °C. 4-Hydroxytamoxifen (H7904), 4-thiouridine (T4509), sodium arsenite and thiamet G (SML0244) were purchased from Sigma. Staurosporine (9953) and anti-eIF2α (9722) were purchased from Cell Signaling. Anti-*O*-GlcNAc (RL2, MA1-072), Alexa Fluor 488- or Alexa Fluor 546-labeled secondary antibodies (A21202, A10040) and Hoechst were purchased from Fisher Scientific; anti-eIF4GI (sc-11373), anti-eIF4E (sc-9976) from Santa Cruz; anti-Flag (M2) and β-actin monoclonal antibody (F1804) from Sigma; anti-OGT (11576-2-AP) and anti-G3BP1 (13057-2-AP) from Proteintech; anti-Hsp70 (SPA810) anti-Hsp25 (SPA801) from Enzo Life Sciences; anti-eIF4GI for IF (2858), anti-HSP90 (4874), anti-RPS6 (2217), anti-PARP (9542), anti-eIF4E (9742) and anti-PABP1 (4992) from Cell Signaling; anti-eIF4GI C-terminal and anti-eIF4GII antibodies were kindly provided by Nahum Sonenberg (McGill University)[46]. siRNAs targeting human OGT and mouse PABP1 were purchased from Santa Cruz. Plasmids and siRNA transfections were performed using Lipofectamine 2000 (Invitrogen) according to the manufacturer's instruction.

Plasmids. eIF4GI cDNA was cloned from total RNAs extracted from HeLa cells by RT-PCR. The amplified eIF4GI coding sequence was inserted into pcDNA3.1/myc-his (Invitrogen). For eIF4GI mutants, mutagenesis was performed using the QuikChange II site-directed mutagenesis kit according to the manufacturer's instruction (Stratagene). All plasmids were confirmed by DNA sequencing.

Generation of eIF4GI mutants cell lines by LentiCRISPRv2. LentiCRISPRv2 plasmids targeting eIF4GI and PABP1 were constructed using methods previously described[47,48]. Briefly, complementary oligonucleotides containing the specific sgRNA sequence and overhangs complementary to overhangs generated by BsmBI digestion of LentiCRISPRv2 were annealed to the BsmBI digested LentiCRISPRv2 plasmid to generate the functional transfer vector. Undigested LentiCRISPRv2 plasmid lacking a sgRNA sequence was used for pseudovirus production as a control (Scramble). The sgRNA sequence for eIF4GI S68 is ACTCGGGAGGCTGCACTGCT (antisense); for eIF4GI P700, AGCACCACATCAGTGATATG (antisense); for PABP1, GCAAGCCAGTACGCATCATG (sense). Lentiviral particles were packaged using Lenti-X 293 T cells (Clontech). Virus-containing supernatants were collected 48 h after transfection and filtered to eliminate cells, and target cells were infected in the presence of 8 μg mL^{-1} Polybrene. Cells were selected 48 h later with 2 μg mL^{-1} puromycin. Single-cell suspensions of selected cells were transferred to 96-well plates by serial dilution. Single cells were then expanded and analyzed by PCR amplification of genomic DNA flanking the CRISPR-targeted region. Forward primer for eIF4GI S68: 5′AAGCTTAAGGAGGCCACTTAGCCATCAG-3′; reverse primer for eIF4GI S68: 5′TCTAGAACTACACACTAGGTAACCTGAC-3′; forward primer for eIF4GI P700: 5′AAGCTTAGTACAAGTCAGGTGTGTTTAAG-3′; reverse primer for eIF4GI P700: 5′ TCTAGACTCGGGGGCCCACGGTTGCTG-3′. The insertion or deletion of eIF4GI was identified by DNA sequencing.

Mass spectrometry to map the O-GlcNAcylation sites of eIF4GI. $Ogt^{F/Y}$(mER-Cre) MEFs were treated with heat shock at 42 °C for 1 h followed by recovery at 37 °C for 2.5 h. Cell lysates were then collected followed for eIF4GI immunoprecipitation. Immunopurified eIF4GI was submitted to the Proteomics Facility at Cornell University Institute of Biotechnology for MS. For in-gel trypsin digestion, the 250-kDa protein bands from an SDS–PAGE gel were cut into ~1 mm cubes and subjected to in-gel digestion followed by extraction of the tryptic peptide. The excised gel pieces were washed consecutively in 200 μL distilled water, 100 mM ammonium bicarbonate (ambic)/acetonitrile (1:1) and acetonitrile. The gel pieces were reduced with 70 μL of 10 mM DTT in 100 mM ambic for 1 h at 56 °C, alkylated with 100 μL of 55 mM iodoacetamide in 100 mM ambic at room temperature in the dark for 60 min. After wash steps as described above, the gel slices were dried and rehydrated with 50 μL trypsin (Promega) in 50 mM ambic, 10% acetonitrile (20 ng/μL) at 37 °C for 16 h. The digested peptides were extracted twice with 70 μL of 50% acetonitrile, 5% formic acid and once with 70 μL of 90% acetonitrile, 5% formic acid. Extracts from each sample were combined and lyophilized.

For *O*-linked glycosylation identification, the in-gel tryptic digests were reconstituted in 20 μL of 0.5% formic acid for nanoLC-ESI-MS/MS analysis, which was carried out using an Orbitrap Fusion Tribrid (Thermo-Fisher Scientific, San Jose, CA) mass spectrometer equipped with a nanospray Flex Ion Source coupled with a Dionex UltiMate3000RSLCnano system (Thermo, Sunnyvale, CA). The gel-extracted peptide samples (10 μL) were injected onto a PepMap C-18 RP nanotrap column (5 μm, 100 μm i.d. × 20 mm, Dionex) with nanoViper fittings at 20 μL/min flow rate for online desalting and then separated on a PepMap C-18 RP nanocolumn (2 μm, 75 μm × 25 cm) at 35 °C, and eluted in a 90 min gradient of 5% to 38% acetonitrile in 0.1% formic acid at 300 nL/min. The Orbitrap Fusion was operated in positive ion mode as described previously[49]. The Orbitrap full MS survey scan (m/z 400–1,800) was followed by 3 s 'Top Speed' data-dependent Higher Collision dissociation product ion triggered ETD (HCD-pd-ETD) MS/MS scans for precursor peptides with 2–8 charges above a threshold ion count of 50,000 with normalized collision energy of 32%. Product ion trigger list consisted of peaks at 204.0867 Da (HexNAc oxonium ion) or 138.0545 Da (HexNAc fragment). The ETD reaction time was set at 150 ms and the SA energy was set at 20%. All data were acquired under Xcalibur 3.0 operation software and Orbitrap Fusion Tune Application v. 2.1 (Thermo-Fisher Scientific).

All MS and MS/MS raw spectra from each sample were searched using Byonic v. 2.8.2 (Protein Metrics, San Carlos, CA) using a mouse protein database. The peptide search parameters were as follow: two missed cleavage for full trypsin digestion with fixed carbamidomethyl modification of cysteine, variable modifications of methionine oxidation and deamidation on asparagine or glutamine residues. The peptide mass tolerance was 10 ppm and fragment mass tolerance values for HCD and EThcD spectra were 0.05 Da and 0.6 Da, respectively. Both the maximum number of common and rare modifications were set at two. The glycan search was performed against a list of 78 mammalian O-linked glycans. Identified peptides were filtered for maximum 2% FDR.

Immunoprecipitation. Cells were washed twice with PBS and lysed in lysis buffer A (20 mM Tris-HCl, pH 7.5, 100 mM KCl, 1 mM dithiothreitol, 0.5 mM EDTA, 10% glycerol, 0.5% NP-40). Lysates were spun at 16,000 *g* for 15 min at 4 °C and supernatants were collected and incubated with primary antibody and agarose beads at 4 °C for overnight. Immunoprecipitates were washed four times with lysis buffer A. The washed beads were resuspended in SDS sample buffer (100 mM Tris, pH 6.8, 2% SDS, 15% glycerol, 5% β-mercaptoethanol, 0.1% bromophenol blue), boiled for 5 min and analyzed by immunoblotting.

Fractionation. Cells were washed twice with PBS and lysed in lysis buffer A on ice for 15 min. After spin at 16,000 *g* for 15 min at 4 °C, three volumes of supernatants was mixed with one volume 4× SDS sample buffer and pellets were resuspended in 1× SDS sample buffer, then boiled for 5 min, resolved by SDS-PAGE and processed for immunoblotting.

RNA isolation and RT-qPCR. Total cellular RNA was extracted using the TRIzol reagent (Invitrogen) according to the manufacturer's instruction. Single-strand cDNA synthesis was carried out using the high-capacity cDNA reverse transcription kit (Applied Biosystems) followed by standard PCR reactions. Real-time PCR reactions were performed using Power SYBR Green Master Mix (Applied Biosystems) using a LightCycler 480. Gene expression was normalized to β-actin cDNA levels and calculated as a relative gene expression using the $2^{-\Delta\Delta Ct}$ method. Oligonucleotide primers are as follows: mouse Hspa1a: forward 5′-TGGTGCAGTCCGACATGAAG-3′ and reverse 5′-GCTGAGAGTCGTTGAAGTAGGC-3′; mouse β2 microglobulin: forward 5′-CTGCTACGTAACACAGTTCCACCC-3′ and reverse 5′-CATGATGCTTGATCACATGTCTCG-3′; mouse β-actin: forward 5′-TTGCTGACAGGATGCAGAAG-3′ and reverse 5′-ACTCCTGCTTGCTGATCCACAT-3′. For ribosome profile analysis, quantification of target genes of each fraction was normalized using the reference firefly luciferase. Primers used are forward 5′-ATCCGGAAGCGACCAACGCC-3′ and reverse 5′-GTCGGGAAGACCTGCCACGC-3′.

For zero-distance crosslinking, cells were pretreated with 100 μM 4SU and then treated with heat shock at 42 °C for 1 h, followed by recovery at 37 °C for indicated times. Cells were washed with PBS once and irradiated at 0.15 J cm^{-2} total energy of 365-nm UV light in a Stratalinker 2400. Cells were collected with lysis buffer B (20 mM Tris-HCl pH 7.4, 150 mM NaCl, 5 mM $MgCl_2$, 1 mM DTT, 1% Triton X-100 and 40 U/mL RNase OUT) containing Turbo DNase I (Invitrogen) 25 U mL^{-1}, and then clarified by centrifugation for 10 min at 20,000 *g*, 4 °C. Supernatants were then incubated with primary antibody and agarose beads for 2 h at 4 °C. The beads were washed by lysis buffer B twice, by lysis buffer B containing 0.1% SDS and 0.05% sodium deoxycholate twice, and then by lysis buffer B twice. Washed beads were treated with 1.2 μg μL^{-1} proteinase K at 55 °C for 30 min, followed by RNA extraction and RT-qPCR.

Immunofluorescence staining. Cells grown on glass coverslips were fixed in 3.7% formaldehyde and permeabilized with 0.5% Triton X-100 in PBS. After blocking in 2% BSA in PBS 30 min, fixed cells were incubated with the primary antibody at 4 °C overnight, followed by 1 h incubation at room temperature with Alexa Fluor-labeled secondary antibodies. Cells were then washed with PBS and incubated for 5 min in PBS supplemented with Hoechst to counterstain the nuclei. After final wash with PBS, coverslips were mounted onto slides and viewed using a confocal microscope (Zeiss LSM710) at the Cornell University Institute of Biotechnology.

Stress granules were quantified using ImageJ (https://imagej.nih.gov/ij) as previously described[44]. Briefly, images were randomly acquired in 4 different fields with at least 30 cells per field. Background intensity was subtracted from each image. The plug-in "Analyze Particles" was used to measure the total area of stress granules/total cell area. The stress granule index was determined by computing the total stress granule area in relation to the total cell area for each field and then averaged across all fields.

RNA FISH. RNA FISH was performed as previously described with small modifications[16]. The same set of Stellaris FISH probes, single-labeled (quasar570) oligonucleotides, were synthesized to bind to mouse *Hspa1a* from Biosearch Technologies. MEF cells grown on glass coverslips were fixed in 3.7% formaldehyde and permeabilized with 0.5% Triton X-100 in PBS. Cells were then washed in PBSM 10 min and incubated 60 min at 37 °C in prehybridization solution (20% formamide, 2 × SSC, 2 mg/mL BSA and 200 mM vanadyl ribonucleoside complex). After prehybridization, the hybridization buffer (Biosearch Technologies, SMF-HB1-10) containing probe (125 nM) plus anti-G3BP1 antibody were added to cells and incubated in the dark at 37 °C for 16 h. Cells were then incubated with wash buffer A (SMF-WA1-60) plus anti-rabbit second antibody in the dark at room temperature for 1 h. Wash buffer A was aspirated, cells were washed twice with wash buffer B (SMF-WB1-20) and then coverslips were mounted onto slides with mounting medium containing DAPI and viewed using a confocal microscope (Zeiss LSM710) at the Cornell University Institute of Biotechnology.

Statistical analysis. Results are expressed as mean ± s.e.m. Comparisons between groups were made by two-way ANOVA and unpaired two-tailed Student *t*-test.

Reporting Summary. Further information on experimental design is available in the Nature Research Reporting Summary linked to this article.

Data availability. All data generated or analyzed during this study are included in this published article (and its Supplementary Information files) or are available from the corresponding author on reasonable request.

References

46. Ramirez-Valle, F., Braunstein, S., Zavadil, J., Formenti, S.C. & Schneider, R.J. eIF4GI links nutrient sensing by mTOR to cell proliferation and inhibition of autophagy. *J. Cell Biol.* **181**, 293–307 (2008).
47. Sanjana, N. E., Shalem, O. & Zhang, F. Improved vectors and genome-wide libraries for CRISPR screening. *Nat. Methods* **11**, 783–784 (2014).
48. Shalem, O. et al. Genome-scale CRISPR-Cas9 knockout screening in human cells. *Science* **343**, 84–87 (2014).
49. Thomas, C. J., Cleland, T. P., Zhang, S., Gundberg, C. M. & Vashishth, D. Identification and characterization of glycation adducts on osteocalcin. *Anal. Biochem.* **525**, 46–53 (2017).

nature research

Corresponding author(s): Shu-Bing Qian

Life Sciences Reporting Summary

Nature Research wishes to improve the reproducibility of the work that we publish. This form is intended for publication with all accepted life science papers and provides structure for consistency and transparency in reporting. Every life science submission will use this form; some list items might not apply to an individual manuscript, but all fields must be completed for clarity.

For further information on the points included in this form, see Reporting Life Sciences Research. For further information on Nature Research policies, including our data availability policy, see Authors & Referees and the Editorial Policy Checklist.

Please do not complete any field with "not applicable" or n/a. Refer to the help text for what text to use if an item is not relevant to your study.
For final submission: please carefully check your responses for accuracy; you will not be able to make changes later.

Experimental design

1. Sample size

   Describe how sample size was determined.

   For independent experiments, at least three replicates are conducted. For stress granule (SG) index calculation, 120 YFP positive cells are quantified for each experiment.

2. Data exclusions

   Describe any data exclusions.

   No data were excluded

3. Replication

   Describe the measures taken to verify the reproducibility of the experimental findings.

   Yes, at least three biological replicates

4. Randomization

   Describe how samples/organisms/participants were allocated into experimental groups.

   Independent experiments like immunoblotting cannot be randomized.

5. Blinding

   Describe whether the investigators were blinded to group allocation during data collection and/or analysis.

   Independent experiments like immunoblotting cannot be blinded.

Note: all in vivo studies must report how sample size was determined and whether blinding and randomization were used.

6. Statistical parameters

   For all figures and tables that use statistical methods, confirm that the following items are present in relevant figure legends (or in the Methods section if additional space is needed).

n/a	Confirmed
☐	☒ The exact sample size (*n*) for each experimental group/condition, given as a discrete number and unit of measurement (animals, litters, cultures, etc.)
☐	☒ A description of how samples were collected, noting whether measurements were taken from distinct samples or whether the same sample was measured repeatedly
☐	☒ A statement indicating how many times each experiment was replicated
☐	☒ The statistical test(s) used and whether they are one- or two-sided *Only common tests should be described solely by name; describe more complex techniques in the Methods section.*
☐	☒ A description of any assumptions or corrections, such as an adjustment for multiple comparisons
☐	☒ Test values indicating whether an effect is present *Provide confidence intervals or give results of significance tests (e.g. P values) as exact values whenever appropriate and with effect sizes noted.*
☐	☒ A clear description of statistics including central tendency (e.g. median, mean) and variation (e.g. standard deviation, interquartile range)
☐	☒ Clearly defined error bars in all relevant figure captions (with explicit mention of central tendency and variation)

See the web collection on statistics for biologists for further resources and guidance.

Software

Policy information about availability of computer code

7. Software

Describe the software used to analyze the data in this study.	Microsoft Excel, SigmaPlot, GraphPad Prism, ImageJ

For manuscripts utilizing custom algorithms or software that are central to the paper but not yet described in the published literature, software must be made available to editors and reviewers upon request. We strongly encourage code deposition in a community repository (e.g. GitHub). *Nature Methods* guidance for providing algorithms and software for publication provides further information on this topic.

Materials and reagents

Policy information about availability of materials

8. Materials availability

Indicate whether there are restrictions on availability of unique materials or if these materials are only available for distribution by a third party.	All materials are readily available

9. Antibodies

Describe the antibodies used and how they were validated for use in the system under study (i.e. assay and species).	anti-eIF2 alpha (9722) was purchased from Cell Signaling. Anti-O-GlcNAc (RL2, MA1-072), Alexa Fluor 488 or 546 labeled secondary antibodies (A21202, A10040) and Hoechst were purchased from Fisher Scientific; anti-eIF4GI (sc-11373), anti-eIF4E (sc-9976) from Santa Cruz; anti-Flag (M2) and beta-actin monoclonal antibody (F1804) from Sigma; anti-OGT (11576-2-AP) and anti-G3BP1 (13057-2-AP) from Proteintech; anti-Hsp70 (SPA810) anti-Hsp25 (SPA801) from Enzo Life Sciences; anti-eIF4GI for IF (2858) , anti-HSP90 (4874) , anti-RPS6 (2217), anti-PARP (9542), and anti-eIF4E (9742), and anti-PABP1 (4992) from Cell Signaling; anti-eIF4GI C-terminal and anti-eIF4GII antibodies were kindly provided by Dr. Nahum Sonenberg (McGill University).

10. Eukaryotic cell lines

a. State the source of each eukaryotic cell line used.	MEF/Ogt F/Y(mER-Cre), MEF/Ogt F/Y(GFP), MEF, HeLa
b. Describe the method of cell line authentication used.	Cell lines are not yet authenticated
c. Report whether the cell lines were tested for mycoplasma contamination.	Cell lines are not yet test for mycoplasma contamination
d. If any of the cell lines used are listed in the database of commonly misidentified cell lines maintained by ICLAC, provide a scientific rationale for their use.	No misidentified cell lines were used

Animals and human research participants

Policy information about studies involving animals; when reporting animal research, follow the ARRIVE guidelines

11. Description of research animals

Provide all relevant details on animals and/or animal-derived materials used in the study.	No animal were used

Policy information about studies involving human research participants

12. Description of human research participants

Describe the covariate-relevant population characteristics of the human research participants.	The study did not involve any human research participants